Development of a Compact Acquisition System for Touch Location on a Conformable Monoport Distributed Sensor

Nissem Selmene[1, 2], Sylvain Blayac[1], Muriel Muller[2] and Ghalid Abib[2]

1. Flexible Electronics Department—PS2, Mines Saint Etienne, Gardanne, France

2. Electronics and Physics Department, Télécom SudParis, Evry, France

Abstract: A compact acquisition system developed for a flexible large area monoport tactile surface is presented in this paper. This sensor requires a single port connection and avoids complicated matrix acquisition system and multiplexing. The tactile surface is based on a coplanar transmission line printed on a large area flexible substrate. Touching the waveguide generates a reflected signal. A harmonic analysis of this reflected signal at the line input port allows locating the touch event. A compact and low complexity acquisition system has been developed in order to demonstrate the principle and evaluate the feasibility of its integration on the sensor. Theoretical background, design and measurements on the overall sensor are exposed. The acquisition circuit imperfections have been demonstrated experimentally and correction methods have been proposed and implemented. Results are presented, and to assess the precision of the compact acquisition system, they are compared to reference measurements made with a Vector Network Analyzer.

Key words: Coplanar waveguide, flexible touch sensor, touch location, phase detector, Wheatstone bridge, reflectometry, harmonic analysis.

1. Introduction

A tactile sensor detects events related to a variation of local physical quantities (pressure, dielectric constant, electrostatic perturbation…) and locates these events on a surface [1]. Nowadays, sensitive surfaces are widely used for the development of new innovative usages, notably, making touch and gesture sensing, related to inanimate objects, and also, human body and liquids [2].

A good understanding of physical interaction between humans or objects and electronics world is required and large research fields remain to be explored.

To date, various technologies have been developed using diverse approaches. Resistive touch sensor, exploits pressure to complete separated electronic circuits; optical ones are made by a network of

photo-detectors sensitive to the daylight intensity [3]; ultrasonic sensors use piezo-electric actuators for interfacing with electronics, acoustic wave is injected and when a touch occurs a part of this signal is absorbed [4, 5]. Among those techniques, capacitive sensing [6-8] remains the most popular. It is based on a very straightforward coupling between electrostatics and electronics, with very simple and low-cost transducers: electrode arrays directly made on thin films. Skin contact, or its presence in the vicinity of metal planes induces a change in the inter electrode capacitance their capacitance. Overall sensor is generally made of a matrix of electrodes. They are addressed through an array of X-Y interconnection lines. The location process is made by indexing each event to its associated connection lines.

Increasing the size of the tactile surface, to potentially several square meters, makes this matrix-based location method more complex and expensive because of high interconnection and multiplexing complexity. The

Corresponding author: Nissem Selmene, Ph.D., research fields: radio frequency and microelectronics.

concept presented here offers the advantage of a single port connection, whatever the size of the device [9]. The sensing device is based on a transmission line. A touch event causes a change in local characteristic impedance of the waveguide, generating a reflection of signal towards the input port.

The location principle, based on harmonic analysis, using VNA (Vector Network Analyzer) measurement at the input port has been presented previously [9]. The objective of this work is put on the study and demonstration of making the same detection and location function, with a compact, low cost, on-pad integrated solution.

In the following, sensor principles and structure are first presented. The second part is focused on the acquisition system and describes design, calibration and experiments made on the two blocks of this system. Final section is dedicated to the comparison between fully integrated system results and reference VNA measurements.

2. Sensor Principles and Structure

2.1 Harmonic Detection and Location Method

The touch-sensing surface is based on a CPW (coplanar waveguide) made on a flexible substrate (Fig. 1).

A transmission line is characterized by its characteristic impedance (Z_c). A good signal transmission is insured when the line is well adapted.

Touching the CPW induces a change in local impedance so that a portion of the incident signal is backscattered towards the input port. This signal is named reflected wave.

The traditional method used to locate an event

(impedance change, or defect) on a waveguide is TDR (Time Domain Reflectometry), which consists in measuring the time-delay between input and reflected pulse [10]. The main drawback of this technique is that, when used on small distances, it requires a very high bandwidth (GHz) in order to be compatible with very small delay times.

We developed a method called HDL (Harmonic Detection and Location) working at relatively low frequency and small bandwidth in comparison to TDR. This technique allows detection and location in the range of 10-300 MHz. HDL is based on the measurement of the input reflection coefficient phase and subsequent extraction of event position.

A model of the line with a length l, and a touch event occurring at position d can be modeled as described in Fig. 2a, Z_c representing the characteristic impedance and Z_l the impedance of the object at the origin of the event. The second part of the line, which is matched at its end, can be simplified as a load impedance Z_c, as shown in Fig. 2b. From the input port, the whole system can thus be represented as a line of length d, loaded by an impedance Z_p corresponding to the equivalent load impedance.

Fig. 1   Photograph of the flexible touchpad.

(a)   (b)

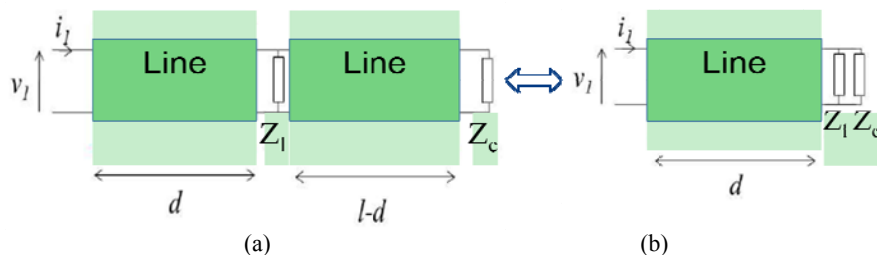Fig. 2   Model of a waveguide with an event occurring at position d.

Considering a lossless transmission line, the input reflection coefficient can be written as:

$$\Gamma_{in} = \Gamma_d e^{j\varphi} \tag{1}$$

with

$$\Gamma_d = \frac{Z_p - Z_c}{Z_p + Z_c} \tag{2}$$

and

$$\varphi = -2\beta d = -2\pi \frac{2d}{\lambda} = -2\pi \frac{2d}{V_\varphi} f \tag{3}$$

where β is the propagation coefficient, λ and f are respectively the wavelength and frequency of the input wave, and V_φ is the phase velocity of the line. When varying the input wave frequency, λ is modified but the delay between input and reflected wave remains constant. A plot of the phase versus frequency exhibits a periodicity f_0, defined as the fundamental frequency for which the phase φ is null (Fig. 3).

f_0 can be expressed as:

$$f_0 = \frac{V_\varphi}{2d} \tag{4}$$

For each multiple frequency f_n ($f_n = n f_0$), the phase φ is zero. Thus, the difference Δf between two frequencies f_n and f_{n+1} is also equal to f_0. So that, extracting Δf in a frequency range allows extracting, the event position, since V_φ is a constant only depending on the waveguide parameters.

We can see in Fig. 3 that there is a clear correlation between Δf and the slope of $\varphi(f)$. We can write:

$$\frac{\delta\varphi}{\delta f} = \frac{\Delta\varphi}{\Delta f} = \frac{2\pi}{\Delta f} = \frac{2\pi.2d}{V_\varphi} \tag{5}$$

Hence, knowing V_φ, the distance d can be determined from the following Eq. (6):

$$d = \frac{\delta\varphi}{\delta f} \frac{V_\varphi}{4\pi} \tag{6}$$

As a result, theoretically, only two measurements of φ at two frequency points are necessary. Thus, the acquisition system can operate with a very narrow bandwidth and does not require high speed acquisition electronics. HDL method requires hardware capable of extracting input reflection coefficient at input port and measuring its phase. The global sensor structure is described in the following part.

2.2 Sensor Structure

2.2.1 Overview

The structure of the complete sensor is presented in Fig. 4. It is composed of:

• A touchpad (touch-sensing surface): a 50 characteristic impedance CPW printed on a flexible substrate.

• An acquisition system: consists of two blocks, the first one performs the separation between incident and reflected waves and the second the extraction of phase φ.
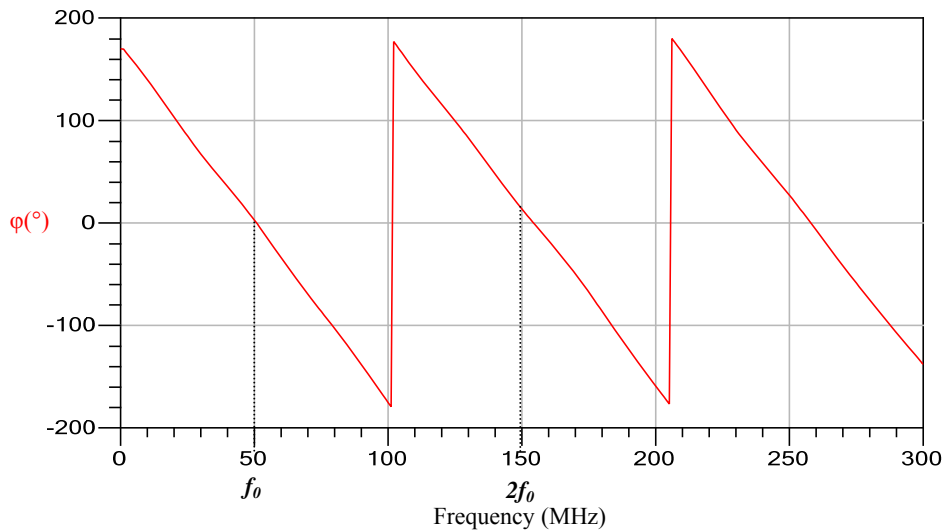

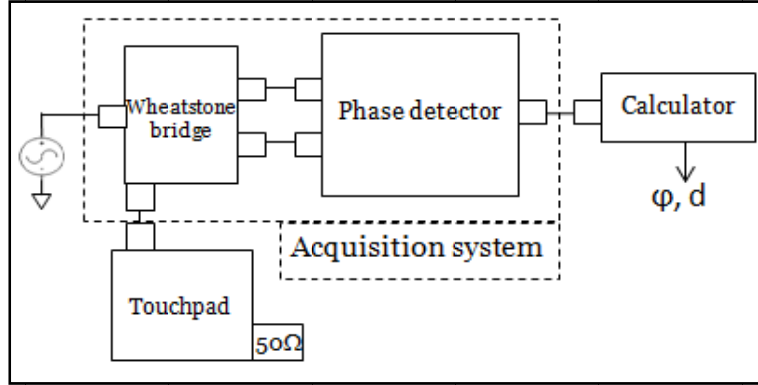Fig. 3   Phase as a function of frequency.

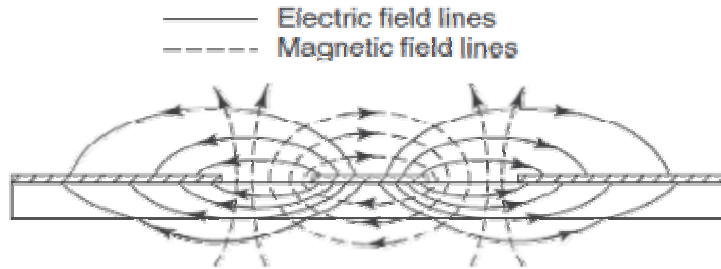**Fig. 4 Schematic of the entire sensor.**

Fig. 5 Field lines in for a CPW line.

• A calculator: implements HDL algorithm.

Each block is detailed hereafter.

2.2.2 Touchpad

The touchpad is a 50 Ω CPW line made with aluminum conductors on a 50 μm thick PET (Poly Ethylene Terephtalate) substrate. The waveguide is designed following three criteria:

• 50 Ω characteristic impedance.

• Sensitivity of the touchpad: Unlike microstrip waveguides, where field lines are confined in the substrate, CPW exhibit field lines outside the substrate which make it more sensitive to the environment (Fig. 5).

• Horizontal design: Total width of the waveguide has to be lower than the average width of a finger, and the coverage of the surface has to be optimized.

The fabricated touchpad, shown in Fig. 1, has a 20 cm × 20 cm lateral and a 1.7 m long CPW with 100 μm gap between central conductor lateral ground lines.

2.2.3 Detection Bridge

Fig. 6 represents a Wheatstone bridge where three 50 Ω resistances (Z_c) are used and the fourth, Z_D is made of the touchpad itself.

In "no event" configuration, the touchpad is matched and its input impedance is equal to Z_c, the bridge is balanced and the differential voltage V_{AB} is equal to zero. Touching the pad causes a variation of the touchpad impedance and creates a differential voltage, it is shown in the following that Γ_{in} can be extracted from V_{AB}.

$$V_{in} = V_C - V_D \tag{7}$$

and

$$V_{out} = V_{AB} = V_A - V_B \tag{8}$$

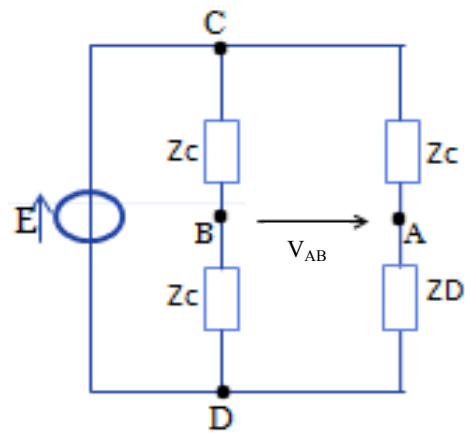According to Millman algorithm:

Fig. 6 Wheatstone bridge circuit.

$$V_A = \frac{V_D Z_C + V_C Z_D}{Z_C + Z_D} \qquad (9)$$

and

$$V_B = \frac{V_D + V_C}{2} \qquad (10)$$

Replacing V_A and V_B by their expression in Eq. (8), we get:

$$V_{out} = \frac{(Z_D - Z_C)(V_C - V_D)}{2(Z_D + Z_C)} = \frac{1}{2}\Gamma_D(V_C - V_D) = \frac{V_{in}}{2}\Gamma_D \quad (11)$$

In our case, the node D is connected to the ground, so, we can use the equality:

$$V_B = \frac{V_{in}}{2} \qquad (12)$$

Moreover, the input reflection coefficient of the touchpad is expressed as:

$$\Gamma_D = \frac{Z_D - Z_C}{Z_D + Z_C} \qquad (13)$$

So that, reflection coefficient can be expressed as follows:

$$\Gamma_{in} = \frac{V_{AB}}{V_B} = \frac{V_A - V_B}{V_B} \qquad (14)$$

where V_B is the incident wave and V_{AB} is the reflected one.

For a best bridge operation, it has to be in a good balance. So, before its realization, a circuit modeling with ADS software has been performed to guarantee a minimum error. S-parameters characterization and simulations have proven a good correspondence between VNA results and simulated bridge ones.

2.2.4 Phase Detection

(a) Principle

The function of the phase detector is to provide a precise value of the reflection coefficient phase φ. Phase detection can be performed using a multiplication operation between the two analyzed waves:

$$V_s = V_1 \times V_2 = A1.A2.\cos(wt + \varphi_1).\cos(wt + \varphi_2)$$

$$= \frac{A1.A2}{2}(\cos(2wt + \varphi_1 + \varphi_2) + \cos(\varphi_1 - \varphi_2)) \quad (15)$$

In Eq. (15) the phase shift $\Delta\varphi = (\varphi_1 - \varphi_2)$ appears. It can be extracted as following:

$$\Delta\varphi = \cos^{-1}\left(\frac{average(Vs)}{module(Vs)}\right) \qquad (16)$$

(b) Integrated phase detector

The two output voltages V_A and V_B from the Wheatstone bridge are connected to an integrated phase detector (Analog Devices AD8302) [11]. This circuit delivers two DC output voltages VPHS and VMAG that are related respectively to the phase shift φ and the magnitude ratio ρ of the two input voltages. φ is expressed by Ref. [11]:

$$\varphi = D.VPHS + E \qquad (17)$$

where D and E are parameters given in Ref. [11].

2.2.5 Location Algorithm

The location algorithm is implemented in the calculator (Fig. 4). It allows extracting phase φ, then, the slope $\varphi(f)$ is exploited to deduct the position d, from Eq. (6).

3. Experiments

3.1 Reference Measurements (VNA Method)

The first experimental tests are performed with a VNA to validate the HDL method, and to serve as a reference. A one meter long cable is added to the experimental setup, between the touchpad and the VNA, in order to have a minimum delay between input and reflected wave and thus obtain reasonable values of Δf. The total propagation time including the cable and CPW on touchpad is:

$$t_d = \frac{2}{\Delta f} \qquad (18)$$

From this value, the time delay associated to the cable is subtracted to get the propagation time in the line (t_d), then, the event position is calculated using:

$$d = V_\varphi.t_d \qquad (19)$$

The precision of location is evaluated by measurement of the linearity of the event position d as a function of t_d. This curve is obtained by extracting d from the slope of $\varphi(f)$ at different event locations (an event is in this case a touch of the line a distance d). Results are shown in Fig. 7.

Results have assessed the relevance of HDL method by obtaining an excellent linearity of this curve.

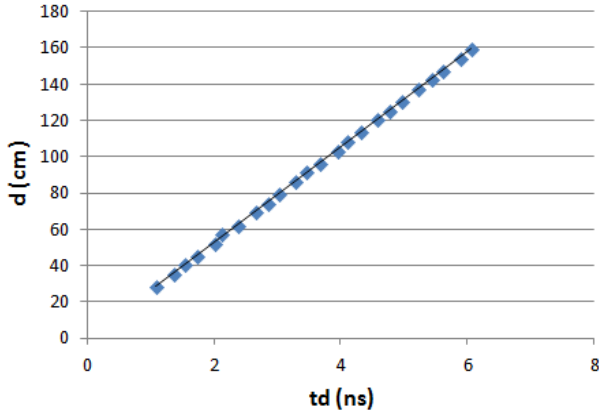Least square method is used to extract the individual

Fig. 7   Position d as a function of the propagation time using a VNA.

errors from the local deviation between the line fit and the local measurement.

A location error histogram is represented for different touch positions (Fig. 12). The maximum error is 1.8 cm corresponding to a percentage of 1.06% over the 170 cm waveguide length.

3.2 Integrated Measurements Performance Evaluation

3.2.1 First Acquisition Block: Wheatstone Bridge

(a) Measurements

A second measurement has been performed using the HDL method with the realized Wheatstone bridge (Fig. 8), and an oscilloscope connected to A and B outputs. The measurement setup is represented by Fig. 9.

Γ_{in} is then calculated (Eq. (14)) and its phase is plotted as a function of frequency. Next, we determine the propagation time (Eq. (18)) and represent d as a function of t_d as shown in Fig. 10.

Fig. 10 shows deterioration in the linearity of the curve that was perfect in the case of reference measurements done with the VNA (Fig. 7). Moreover, maximum error increases reaching a maximum of 5 cm (Fig. 12). This is due to the insertion of the bridge.

In order to reduce this effective error, a calibration method has been developed and is presented in the following.

(b) Implementation of bridge calibration

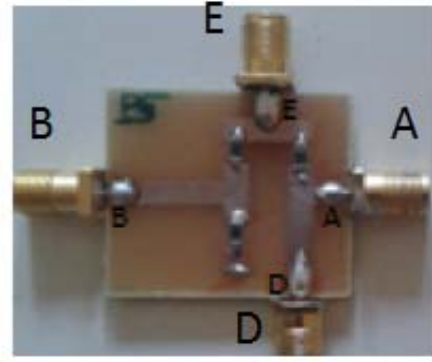The insertion of Wheatstone bridge introduces some

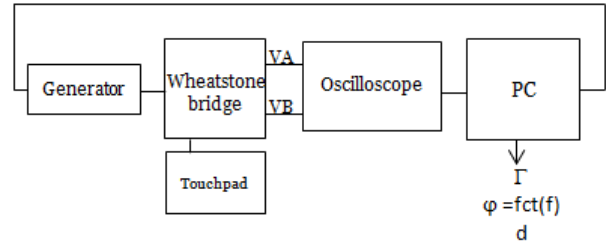Fig. 8   Photography of the realized Wheatstone bridge.
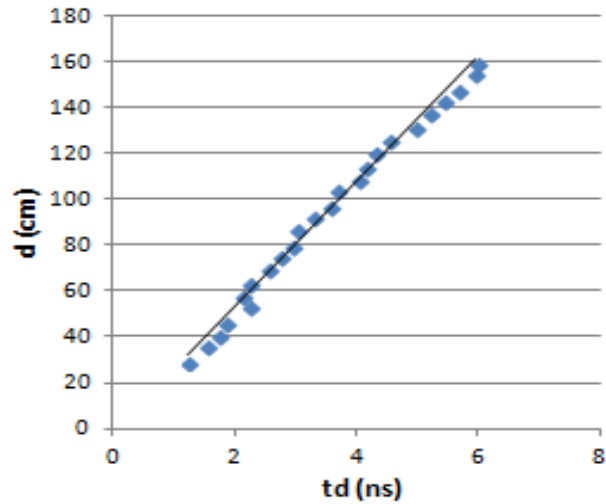

Fig. 9   Wheatstone bridge measurement setup.

Fig. 10   Position d as a function of the propagation time using a non calibrated bridge.

defects due to mismatches in the connection lengths and slight variations of its resistors. It is proven experimentally that these imperfections of the circuitry result in additional measurement errors (Figs. 10 and 12).

A new calculation of the reflection coefficient is made according to the following formula:

$$\Gamma_{in} = A \frac{V_B + B V_A}{V_B + C V_A} \qquad (20)$$

where A, B and C are calibration parameters. They are determined with a SOLT (Short Open Load Thru) calibration procedure, with known elements.

Using the calibration procedure Eq. (20), new measurements have been performed. Results are shown in Fig. 11 where d as a function of t_d is shown for the calibrated bridge case.

We notice that on the curve (Fig. 11) linearity improves when we calibrate the Wheatstone bridge, and, the maximum error value decreases by 2 cm. It is now equal to 3 cm, which represents 1.76% of the total length.

(c) Bridge results summary

From three cases represented characteristic curves (Figs. 7, 10 and 11), a location error histogram can be elaborated for some of the tested touch positions. This histogram allows evaluating different measurement methods by comparing their location errors.

This errors histogram validates bridge calibration method. It is clear, as shown in Fig. 12, that calibrating the bridge reduces considerably locating errors. So that, calibrated Wheatstone bridge, shows good performances in comparison with VNA.

Now, for all tested positions, after extracting errors from each characteristic curve, a frequency count analysis has been performed for the three measurement configurations (Fig. 13).

All the distributions are centered on zero. The standard deviation is 0.84 cm for VNA measurements. It increases up to 4.35 cm when the bridge is inserted. Introducing the calibration method allows reducing this error to 2.9 cm.

This standard deviation can be a criterion of performance evaluation. Lower it is, more errors are closer to zero.

In the following, we will work with the calibrated Wheatstone bridge and replace the oscilloscope by a phase detector to form the entire integrated acquisition system.

3.2.2 Second Acquisition Block: Phase Detector

(a) Measurements

In this setup (Fig. 14), we replace the oscilloscope by the AD8302 phase detector and two voltmeters. Our acquisition system is, now, entirely tested experimentally with its two blocks. The DC outputs of the phase detector are exploited to determine the phase value for each generated frequency (Eq. (17)), and the phase as a function of input frequency is then plotted.
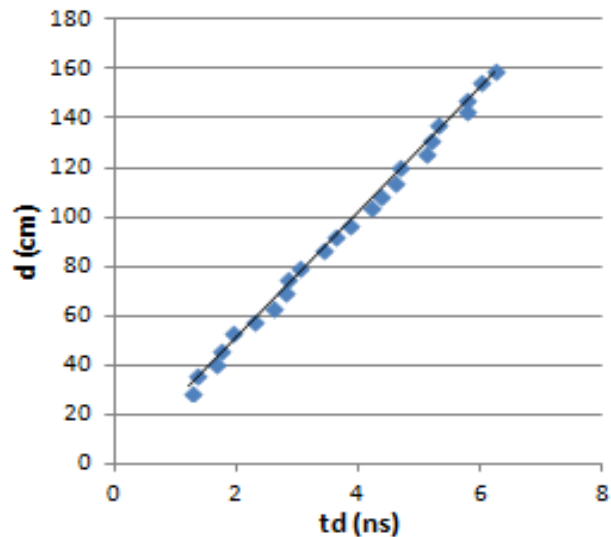

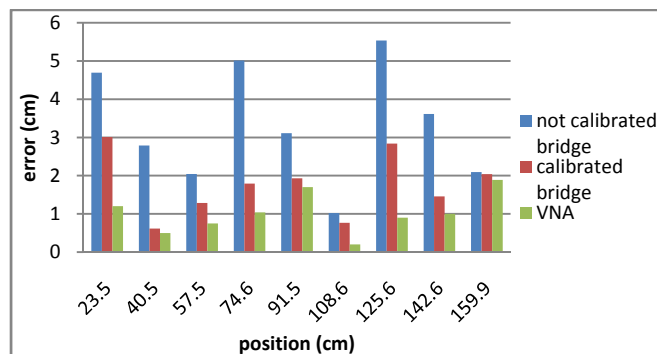**Fig. 11 Position d as a function of the propagation time using calibrated bridge.**

Fig. 12 Error histograms for calibrated and non-calibrated Wheatstone bridge compared to VNA.
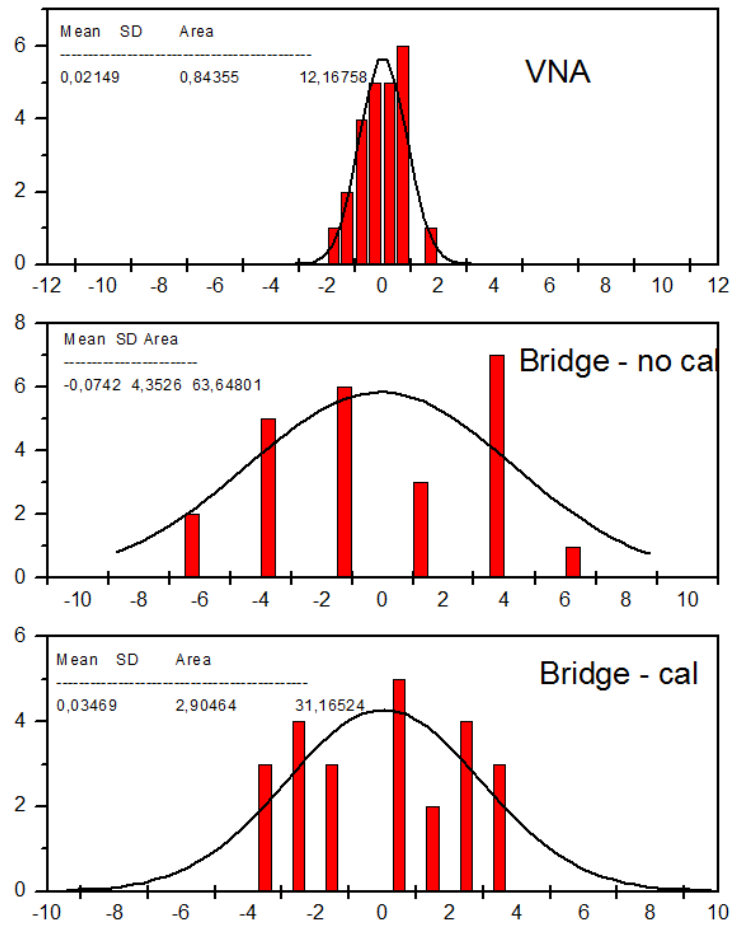
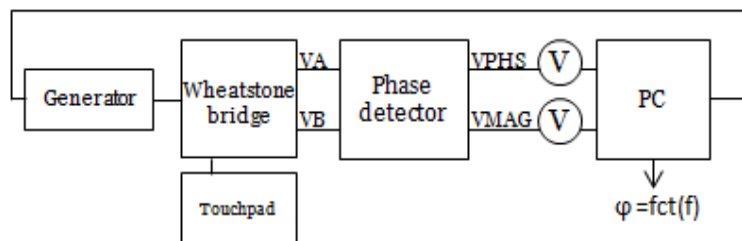Fig. 13 Error histograms (frequency count/error in cm).

Fig. 14 Insertion of the phase detector in the measurement setup.

(b) Implementation of the phase detector calibration

Measurements are performed at different input signal frequencies. The phase detector presents a variation of D and E coefficient, leading to a distortion of phase curves. This problem is solved by calibrating the phase detector for each frequency value and replacing theoretical Eq. (17) by real calibrated one as follows:

$$\varphi(f) = D(f).VPHS + E(f) \qquad (21)$$

where D and E are frequency dependent calibration parameters.

(c) Results

The phase detector calibration improves notably the phase curve linearity as shown in Fig. 15 and coincides with the VNA reference phase. Fig. 16 presents the error histograms for the non calibrated and calibrated phase detector compared to VNA reference measurement. Hence, for some positions, the error measurement is decreased by 5 cm when calibrating the phase detector. Thus, the maximum error compared the VNA reference measurement is around 3 cm. This assesses the feasibility of a fully integrated acquisition system.
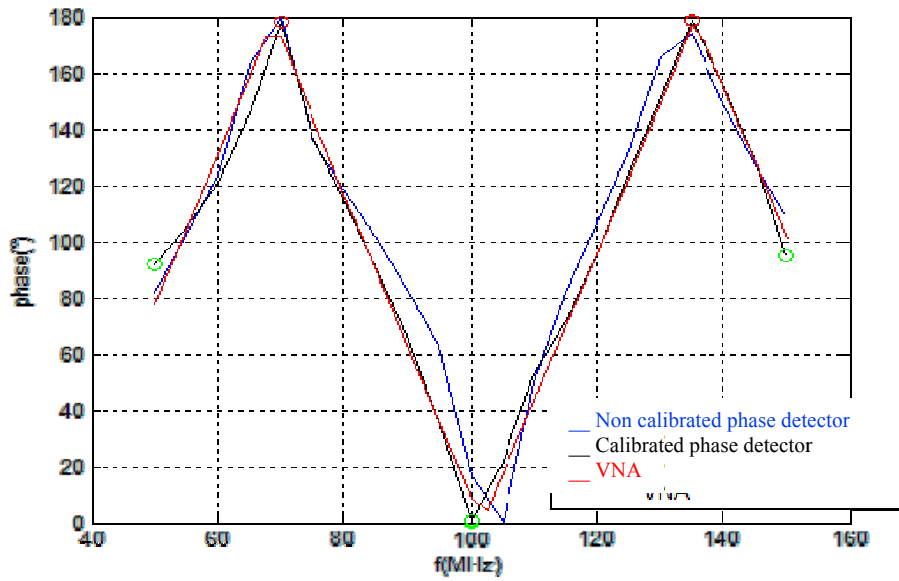
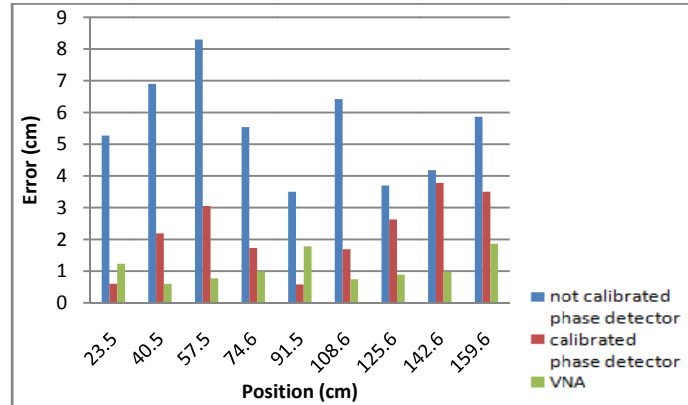**Fig. 15   AD8302 and VNA phase curves comparison.**

Fig. 16   Error histograms for calibrated and non calibrated phase detector compared to VNA.

4. Discussion and Future Work

This work has clearly shown the relevance of HDL method, which assesses the possibility of a location with a precision below 1.8 cm, this indicates that large area touch sensor, in the order of one to several square meters are feasible, with a single port detection, and a very low cost substrate. The use of Wheatstone bridge detection degrades the precision, but considerably reduces the cost and size of acquisition circuit which can be integrated on the touchpad. We have shown that implementing a calibration procedure can help the compensation of error. A second block of the acquisition system has been also validated with its calibration method which corrects linearity problem of the curve of phase. Future work is underway to fully compensate error using an advanced calibration method, allowing compensation of both acquisition system and touchpad defects. This method will rely on a first measurement of S parameters for various event positions which will serve as a reference database. Correction matrices will thus be determined and systematically used to correct the results. Additional work on hardware will include the improvement of the calibration method of the phase detector to correct the edges defects, moreover, the integration of a microcontroller into the acquisition system is planned in order to ensure a real time touch location.

5. Conclusion

A new concept of compact acquisition system has been developed for a large area monoport tactile surface. The touchpad is a coplanar waveguide line printed on a flexible substrate and connected to the acquisition system at the unique input port. HDL method has been validated with VNA and then implemented in a compact system. A system composed of two blocks, a Wheatstone bridge to separate reflected and incident waves and a phase detector to extract the phase shift between them is presented and evaluated. The use of these components allows performing the extraction of touch position, with no need of complex and expensive equipment (VNA), at the price of a certain degradation of precision. Applying a calibration method for each block allows decreasing significantly the location error.

Future work is underway to improve the second block calibration and to allow compensation of the entire sensor defects and reducing location errors. Moreover, an integrated and compact version of the acquisition system is investigated using a Voltage Controlled Oscillator (VCO), the phase detector, and a microcontroller which implements the location algorithm.

References

[1] Tsuji, S., and Kohama, T. 2013. "A tactile and Proximity Method for 3D touch screen based on Capacitance Measurements." *SICE.*

[2] Sato, M., Poupyrev, I., and Harrison, C. 2012. "Touché: Enhancing Touch Interaction on Humans, Screens, Liquids, and Everyday Objects." *CHI'12.*

[3] Lee, J.-K., Kim, S.-S., Park, Y.-I., Kim, C.-D., and Hwang, Y.-K. 2010. "In-cell Adaptive Touch Technology for a Flexible E-Paper Display." *Solid-State Electronics.*

[4] Liu, Y., Nikolovski, J. P., Mechbal, N., Hafez, M., and Vergé, M. 2010. "An Acoustic Multi-touch Sensing Method Using Amplitude Disturbed Ultrasonic Wave Diffraction Patterns." *Sensors and Actuators A*: Physical.

[5] Adler, R., and Desmares, P. J. 1986. "An Economical Touch Panel SAW Absorption." *IEEE, AFCS.*

[6] Barrett, G., and Omote, R. 2010. "Projected-Capacitive Touch Technology." *Information Display*: 16-21.

[7] Kim, H.-K., Lee, S., and Yun, K.-S. 2010. "Capacitive Tactile Sensor Array for Touch Screen Application." *Sensors and Actuators A*: Physical.

[8] Kang, S.-K., Jung, T.-H., and Cho, S.-H. "Flexible Touch Screen Panel." US patent 2012/0306777 A1.

[9] Blayac, S., Schreiner, A., Nouaille, M., Dubois, B., and Depoutot, F. 2014. "Single Port, Large Area Touch and Force Sensing: Towards Low Cost Sensitive Printed Surfaces." Intelligent Sensors, Sensor Networks and Information Processing (ISSNIP), IEEE Ninth International Conference.

[10] Wimmer, R., and Baudisch, P. 2011. "Modular and Deformable Touch-Sensitive Surfaces Based on Time Domain Reflectometry." UIST'11.

[11] http://www.analog.com/media/en/technical-documentation/data-sheets/AD8302.pdf.